Data Engineering and Applications

Research Paper

Accelerating Quantum Chemistry Simulations Using GPU-Optimized Deep Reinforcement Learning Algorithms

Marek Zielinski[1, *]

[1] Faculty of Electrical and Computer Engineering, Wrocaw University of Science and Technology, 50-370 Wrocaw, Poland
*Corresponding author: marek.zielinski@pwr.edu.pl

Abstract. A distributed deep reinforcement learning framework based on GPU cluster was constructed to solve the computational problems of large-scale quantum chemistry simulation. The framework includes technologies such as parallel strategy optimization, asynchronous gradient update, and dynamic scheduling tasks. Efficient communication algorithms are adopted to maximize the utilization of hardware resources and achieve scaling. Experimental evaluation of representative quantum chemistry problems was performed on a multi-node GPU platform. The results show that the average GPU utilization rate exceeds 92% due to the near-linear scale expansion to 128 GPUs. This improves the simulation throughput and efficiency. The system has good performance and convergence behavior for a variety of workloads. The results show that these GPUs, matched with advanced improved distributed DRL models, can break thru the traditional bottleneck of using supercomputers to solve complex physical and chemical problems, so as to complete all these dazzling and complex molecules faster and better.

Keywords: *quantum chemistry, deep reinforcement learning, GPU clusters, distributed algorithms, high-performance computing, parallel optimization*

Received on 10 September 2024, Accepted on 12 December 2024, Published on 5 Jan2025

Introduction

Quantum chemistry simulations are key to developing new materials at the atomic scale and understanding the properties of molecules. In the development of catalysis, medicine and condensed matter, the simulation around solving the Schrödinger equation of the many-body system is crucial. However, the computational cost of accurate quantum chemical methods such as DFT and CC increases rapidly with the increase of system size, which makes it more difficult to deal with large or strongly correlated systems [1]. Despite the progress made in algorithmic improvements and the introduction of more high-end computing resources, the problem itself remains the biggest obstacle [2]. Traditional methods often struggle to balance computational feasibility with sufficient accuracy, thus requiring fundamentally new computational paradigms [3]. Therefore, scientists are looking for faster and more accurate quantum chemistry methods [4].

The advent of artificial intelligence, especially deep reinforcement learning, has put computational science in a very favorable period [5]. On the other hand, DRL methods have been well applied to solve high-dimensional control problems in molecular design and quantum system optimization [6]. On the other hand, with the rapid development of GPU, large-scale scientific simulation, high throughput and large-scale parallelism become possible [7]. However, GPU-accelerated architecture-based quantum chemistry DRL has not been studied, which means it is a brand new field [8].

This paper presents a complete framework for GPU-optimized DRL algorithms to accelerate quantum chemistry simulations. The difficulties of transferring DRL models to distributed GPU clusters are introduced, and anticorrosion effects are provided for calculation and simulation. To demonstrate this, all representative quantum chemistry tasks to date were evaluated, and algorithmic innovation and parallelization strategies were used. This opens the door to high-fidelity, scalable quantum chemistry simulations and provides a template for the use of AI-driven HPC in computational science.

HPC Infrastructure for Quantum Chemistry

GPU Cluster Architecture

Current GPU clusters can support computational frameworks for quantum chemistry calculations. These groups typically consist of many interconnected nodes, each with a large number of high-power GPUs, a large amount of nearby memory, and many CPU cores. Fast GPU-GPU and GPU-CPU interactions are achieved within a node via PCIe or NVLink links, while fast fabrics such as InfiniBand support communication between nodes. The structure of this hierarchy is designed to break down large quantum chemistry problems into smaller subproblems. It also allows electronic structure methods to meet large memory and parallelism requirements. Thru intelligent task assignment and resource scheduling, the hardware utilization rate is higher, there is no idle cycle, and the throughput is higher. Because of the large data traffic and the fact that quantum chemistry calculations are often iterative linear algebra tasks, the basic architecture of the GPU cluster is a key factor affecting scalability and simulation efficiency [9]. Figure 1 shows the structural layout and functions of a common GPU cluster in quantum chemistry. as well as key issues such as node connection, memory hierarchy, and data transfer methods between GPUs and CPUs.

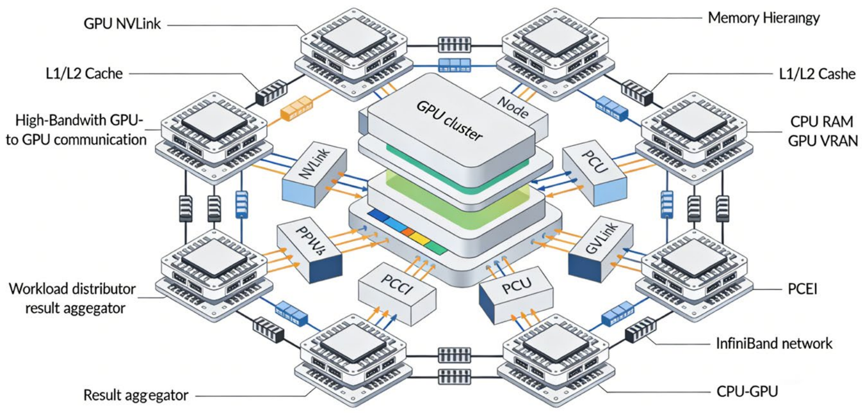

Figure 1. GPU cluster architecture for quantum chemistry simulations.

Figure 1 shows how modern quantum chemistry simulations can achieve high throughput and scalability. This makes sense when all the GPU and CPU nodes are mapped in the visualization. By understanding the arrangement of the physical and logical parts, We will have a clearer understanding of how everything is connected. Multi-core CPUs and high-performance GPUs are integrated with each other in each node, and data movement and calculation within the node are realized thru NVLink or PCIe connection. Distributed workloads such as quantum chemistry require inter-node communication via fast fabrics such as InfiniBand. This architecture describes how the algorithm is implemented thru hardware. This is not just for hardware engineers; the designers of computational tasks also need to consider how the hardware gets there. The diagrams are used to discuss topics such as clustering, awareness scheduling, M HoO, and communication protocol selection. Understanding these architectural connections is critical to locating bottlenecks and opportunities for speedup, which will be examined carefully in the rest of this study.

As simulations grow in size and challenge, the way different parts communicate with each other becomes more complex and difficult to improve. Large-scale quantum chemistry simulations produce a large number of different traffic patterns, so attention needs to be paid to the location of nodes and the network topology to avoid conflicts and excessive message arrival times. This is becoming more difficult with the introduction of exascale computing architectures due to the large increase in the number of GPUs and nodes. To support current and future generations of quantum chemistry workloads, effective cluster design requires anticipating future scalability needs and providing flexible high-bandwidth interconnects [10].

Network and Storage Considerations

Network topology and storage solutions are closely related to the efficiency of distributed quantum chemistry simulations. For the common all-to-all communication pattern used by advanced quantum chemistry algorithms, various topologies (such as fat tree, torus, and dragonfly) can greatly affect bandwidth and latency. If the network is not designed properly, it may lead to congestion or contention; in addition, the parallel performance will be severely affected as the system size increases. In terms of storage, quantum chemistry simulations lead to a large load of checkpoints, intermediate results, and a large number of I/O files. Parallel file systems such as Luster and GPFS provide support for bandwidth and reliability. Therefore, supporting high-throughput, fault-tolerant quantum chemistry workflows require precise integration of network and storage infrastructure [11]. Figure 2 shows the network topology and bottleneck visualization. The graph shows how data moves between nodes, where the congestion points are, and how the parallel file system is connected to the cluster.

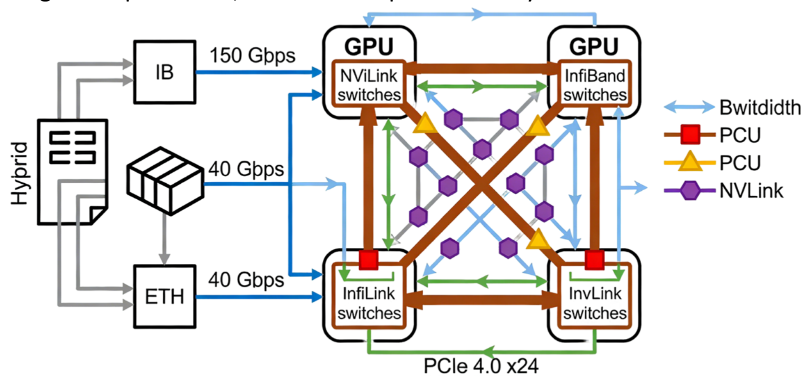

Figure 2. Network topology and bandwidth bottlenecks in a multi-node GPU cluster.

As noted, the efficiency of data transfer depends on the network design and possible congestion points. These are used to select storage systems and communication protocols, which is critical to obtaining good performance for large-scale quantum chemistry workloads.

When starting to use larger scale calculations, communication between nodes can become an issue, especially for collective operations that require coordination across multiple processes. Network topology affects raw bandwidth and the efficiency of collective operations common in quantum chemistry codes [12]. To avoid running out of storage space, especially when viewing or writing a large number of files at the same time, such as high-speed throughput when processing thousands of files, the storage must keep up with the progress of the calculation work [13].

Parallel Computing Paradigms

Efficient quantum chemistry simulations on GPU clusters depend on the chosen parallel computing paradigm. Parallel efficiency (η) and speedup (S) are two main indicators of scalability.

$$\eta - \frac{T_1}{N \cdot T_N}$$
$$S - \frac{T_1}{T_N} \qquad \text{Eq. (1)}$$

In Eq.(1), T_1 is the execution time on a single node, T_N is the execution time on N nodes, η is the fraction of ideal performance retained, and S is the speedup obtained by parallelization. Hybrid models are often used in quantum chemistry codes, which use MPI, OpenMP, CUDA, or OpenCL device-level parallelism to improve computational throughput. For example, fine-grained tasks such as tensor contraction will be handled by GPUs, while more complex tasks such as domain decomposition will be handled by nodes. Despite these approaches, issues such as load imbalance, communication overhead, and synchronization penalties can hinder scaling. In the past few years, task-based asynchronous communication and runtime communication have emerged, which may allow more adaptive and robust parallel operations [14].

Amdahl's law provides a theoretical maximum speed up for parallelization. It shows that the more resources are added, the smaller the gain is when some parts of the calculation are still completed sequentially [15]. The flexibility, adaptability, and energy efficiency of exascale computing initiatives will allow simulations to be addressed thru the co-design of algorithms and system software [16]. Future progress in quantum chemistry simulations will depend on the combination of algorithms and hardware architectures.

Scalable DRL Algorithm Development

Distributed Training Strategies

To make deep reinforcement learning (DRL) as complex as quantum chemistry simulations, a scaling approach is needed. This scaling approach requires the use of distributed systems, where policy and value networks are trained in parallel across multiple GPUs and nodes. From the perspective of quantum chemistry, distributed DRL can be regarded as a method that utilizes data and modeling parallelism to accelerate convergence and improve sample utilization. Figure 3 shows the complex workflow of distributed DRL training, demonstrating the interaction between the environment simulator, worker nodes, and the global parameter server. In the quantum chemistry environment, each worker node independently samples trajectories, calculates gradients, and asynchronously updates global model parameters.

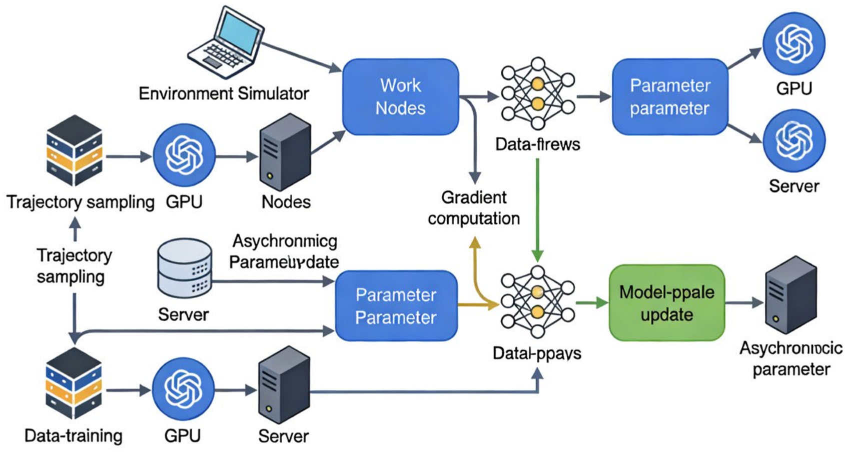

Figure 3. Workflow of distributed DRL training for quantum chemistry simulations.

Figure 3 shows the process of distributed DRL training in the quantum chemistry simulation task. The figure shows how the environment simulator, the distributed worker nodes, and the large parameter server work together in parallel reinforcement learning. Each worker operates independently, interacting with the quantum chemistry environment, producing experience trajectories, computing gradients, and occasionally synchronizing with the global model. This flowchart of asynchronous updates and parallel sampling helps to illustrate the scalability and sample usage of the model. As a conceptual anchor for subsequent chapters of algorithmic innovation (such as adaptive scheduling and communication optimization). Based on this workflow, we show where the gradient flow and data flow, as well as data and parameter and work passing, may have bottlenecks. This systematic view is necessary to understand the reasons for the architectural decisions and the performance enhancements that are analyzed in more detail in the rest of this paper.Distributed optimization is formalized by observing the global objective function of policy optimization.

$$J(\theta) = \mathbb{E}_{\tau\sim\pi_\theta}\left[\sum_{t=0}^{T} r_t\right] \qquad \text{Eq. (2)}$$

From Eq.(2), θ represents the parameters of the policy network, τ denotes state-action trajectories, and r_t is the reward at time t. In a distributed setting, the gradient update for each worker i can be written as Eq.(3):

$$\theta \leftarrow \theta + \alpha \sum_{i=1}^{N} \nabla_\theta J_i(\theta) \qquad \text{Eq. (3)}$$

α is the learning rate, N is the number of workers, and $J_i(\theta)$ is the local objective of worker i.

Asynchronous updates such as A3C and IMPALA reduce communication costs and scale by decoupling gradient computation from parameter synchronization [17]. Nevertheless, this randomness due to asynchrony also affects the convergence stability. Global synchronization interval and adaptive learning rate schedule are used for this. In addition, recent studies have shown that the experience replay buffer among all distributed workers helps to implement offline policy learning and improve sample efficiency [18]. With these strategies, distributed DRL frameworks will be able to leverage large-scale GPU clusters for quantum chemistry tasks, which will reduce training time and improve the robustness of the policy. To briefly compare some of the most distributed DRL frameworks for scientific computing. Table 1 lists some algorithms, including features and scalability.

Table 1. Comparison of Distributed DRL Frameworks for Scientific Computing

Framework	Parallelism Type	Synchronization	Sample Efficiency	Scalability
A3C	Data Parallel	Asynchronous	Moderate	Good
IMPALA	Data Parallel	Asynchronous	High	Excellent
Ape-X	Data/Replay Parallel	Asynchronous	High	Good
Synchronous SGD	Data/Model Parallel	Synchronous	High	Moderate

In scientific computing, the landscape of distributed deep reinforcement learning frameworks involves multiple parallelisms, synchronizations, and efficiencies. Whether it is asynchronous update, experience replay or gradient synchronization, the underlying architecture in the framework selection has a significant impact on the scalability and sample throughput in the real world. When deploying DRL at scale on quantum chemistry projects. Asynchronous methods are particularly well suited to complex stochastic environments, allowing for rapid data collection and are generally more robust to lag effects. Synchronous updates allow for tighter convergence guaranties, but are more susceptible to communication delays as the system scales. Therefore, when choosing a framework, one should consider how much hardware can be utilized, how much idle time can be tolerated, and how robust the learning dynamics are. After seeing how the current best solutions work, do something else. Facilitate scientific discovery and high-end RL systems, while aligning algorithms with the special computational loads of high-fidelity quantum chemistry problems.

Load Balancing and Scheduling

Load balancing is very effective for large DRL systems to make full use of their computing resources, especially when simulating heterogeneous quantum chemistry problems, which require different computing loads. In practice, imbalance exists due to the difference in environment complexity and the randomness of RL episode length. To achieve this, the dynamic scheduling algorithm monitors the workload distribution on GPUs and nodes, and dynamically reallocates simulation jobs to prevent hardware from being idle and improve throughput.

The task load distribution of the distributed DRL system is a direct reflection of the scheduling efficiency and balance. Figure 4 shows that each worker node obtains different quantum chemistry simulation tasks according to the real-time load judgment and dynamic scheduling strategy. Ideally, the workload of all GPUs is evenly distributed, which means that no GPU is idle, thus maximizing the system throughput. Under normal scheduling, the results are histogram med. The load distribution is more efficient because the difference in the number of tasks assigned is smaller. Considering quantitative visualization, adaptive scheduling mechanism is also needed in the non-uniform case. This provides a basis for evaluating the use of available resources and the improvement of the entire system.

$$\sigma_{\mathrm{loxd}} - \sqrt{\frac{1}{N}\sum_{i=1}^{N} (L_i - \bar{L})^2} \qquad \text{Eq. (4)}$$

From Eq.(4), where L_i is the workload assigned to worker i and $\bar{L}$ is the average workload.

The scheduling scenario in Figure 4 below shows the actual application of dynamic workload allocation. The question of how to assign tasks to each node to maximize hardware busy time and idle time. The load imbalance rate is a method of measuring load balancing Eq.(5).

$$\gamma - \frac{\max(L_i)}{\bar{L}} \qquad \text{Eq. (5)}$$

For a perfectly uniform system, this value is close to 1. To improve utilization, feedback-based load redistribution, predictive scheduling using recently completed tasks, and dynamic work stealing [19] are often used. A device-aware scheduling algorithm is used to handle the different clusters. The algorithm also considers the memory bandwidth and capability of each GPU and handles tasks based on the number of teeth that the node actually has. The study shows that adaptive scheduling not only greatly increases the overall training throughput, but also reduces the convergence time of the distributed DRL application of molecular simulation [20].

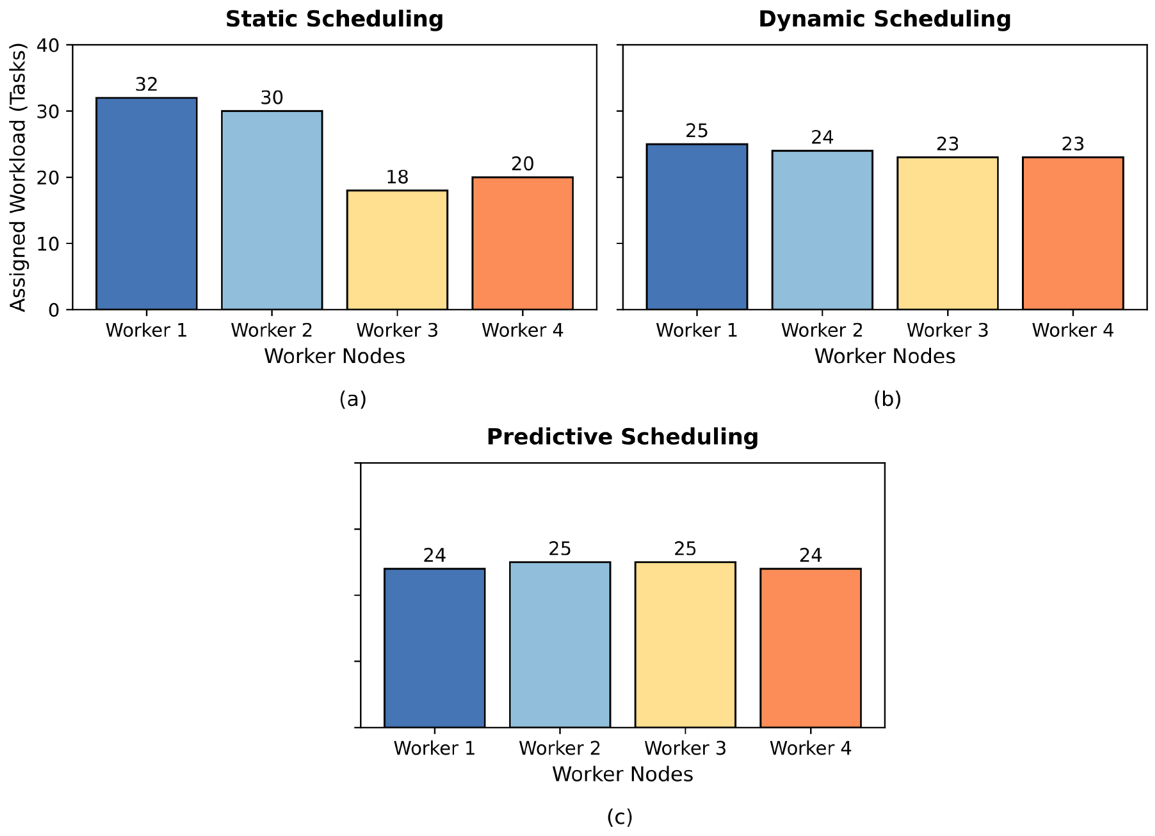

Figure 4. Example of task scheduling and load distribution in a distributed DRL system.
(a) Static scheduling results; (b) Dynamic scheduling results; (c) Predictive scheduling results.

Communication Optimization

Even when scaling to 10 or 100 GPUs, communication costs remain a significant bottleneck for DRL. The frequent exchange of large amounts of gradients, weights, and experience data adds significant latency, which limits parallelism and scalability. To systematically examine these effects, a quantitative analysis was performed, and the latency and bandwidth functions of message size for baseline and optimized communication protocols in distributed DRL training were measured.

The following is a quantitative model of communication latency, Eq.(6):

$$T_{\text{comm}} - \alpha + \beta \cdot S \qquad \text{Eq. (6)}$$

α is the fixed startup latency, T_{comm} is the total communication time, the time per byte transferred, and S is the size of the data transferred. For collective operations such as all-reduce, the communication time can be further analyzed as Eq.(7):

$$T_{\text{all-reduce}} - \log_2(N) \cdot \left(\alpha + \beta \cdot \frac{S}{N}\right) \qquad \text{Eq. (7)}$$

where N is the total number of participating nodes.

To reduce these overheads, more advanced communication methods such as gradient compression, quantization, and communication overlapping computation are becoming increasingly popular [21]. Hierarchical schemes allow groups of GPUs to synchronize locally before synchronizing globally, which helps with scaling. In recent years, improvements in high-speed interconnects and communication libraries such as NCCL and Horovod have improved performance [22]. Therefore, the success of distributed RL in Q-Chem depends on the precise design of the communication protocol and the structure of the DRL algorithm [23].

Evaluation on Large-Scale Simulations

Testhed Configuration

A comprehensive evaluation of the distributed DRL framework was conducted on a high-performance computing (HPC) platform. The experimental testbed consists of 32 compute nodes, each with dual AMD EPYC 7763 CPUs, 64 physical cores, 4 NVIDIA A100 80GB GPUs, NVLink interconnects, and 512GB DDR4. The 200 Gbps high-speed HDR InfiniBand is the basis for inter-node communication, and the Luster parallel file system provides an aggregate throughput of more than 10 GB/s for checkpointing and efficient data exchange. The software stack includes Linux (kernel 5.15), CUDA 11.7, cuDNN 8.x, NCCL, OpenMPI, and Horovod, all of which support large-scale orchestration and distributed GPU activities.

The hardware resources available to the experimental testbed are quantified and summarized in Figure 5. The bar chart shows the number of CPU cores, the number of GPUs, the total amount of system memory, and the InfiniBand bandwidth of the 32-node cluster. This visualization summary shows the powerful computing and communication capabilities of the platform. It can be used as a reference for understanding the scalability results and performance evaluation in the following chapters. According to its resource configuration, the test platform is suitable for benchmarking advanced DRL algorithms that perform well in scientific computing.

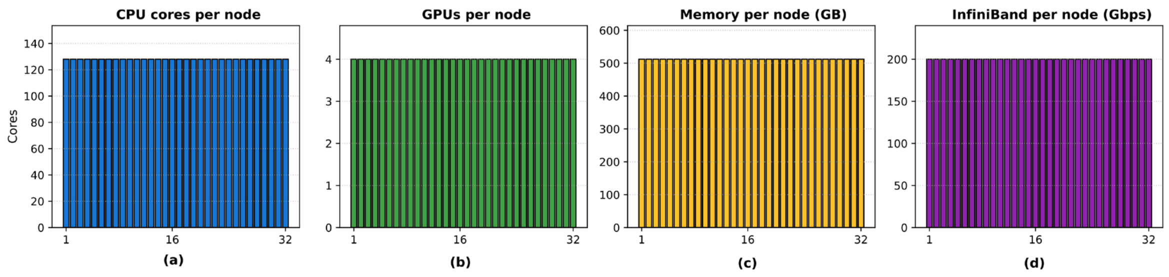

Figure 5. Hardware resources of the experimental testbed.
(a) CPU cores per node; (b) GPUs per node; (c) Memory per node (GB); (d) InfiniBand bandwidth per node (Gbps).

Performance Metrics

To properly measure the various aspects of distributed DRL algorithms, scalability, performance, and resource usage are done thru higher-level metrics. Parallel efficiency (η) refers to the inevitable cost of large-scale communication and synchronization, and the computational speedup brought by increasing the number of nodes. This metric is described as Eq.(8):

$$\eta - \frac{T_1}{N \cdot (T_N + T_{\text{commm}})} \qquad \text{Eq. (8)}$$

T_N is the computation time per node when using N nodes, T_1 is the wall-clock time for single-node training, and T_{comm} is the average communication overhead per iteration. This equation is a reliable indicator of system efficiency because it captures the non-idealities that limit perfect scaling.

Throughput is the consistent rate at which environment steps are processed per second, and is a direct reflection of the system's application in large quantum chemistry simulations. The power of the GPU ensures that no other hardware is left idle due to scheduling and communication inefficiencies.

Scalability Results

Scalability is achieved with 16, 32, 64, and 128 GPUs, each running the same quantum chemistry DRL workload. Figure 6 shows a dual-axis line chart showing the measured speedup (blue line) and parallel efficiency (green dashed line) versus the number of GPUs. The results show that the speedup is almost linear before 128 GPUs, reaching 106.1 times. However, at the maximum, the parallel efficiency is still above 80%. The trend seen here supports a distributed DRL framework that can make good use of more hardware resources, maintain performance, and solve the problem of too much or too little talk and things.

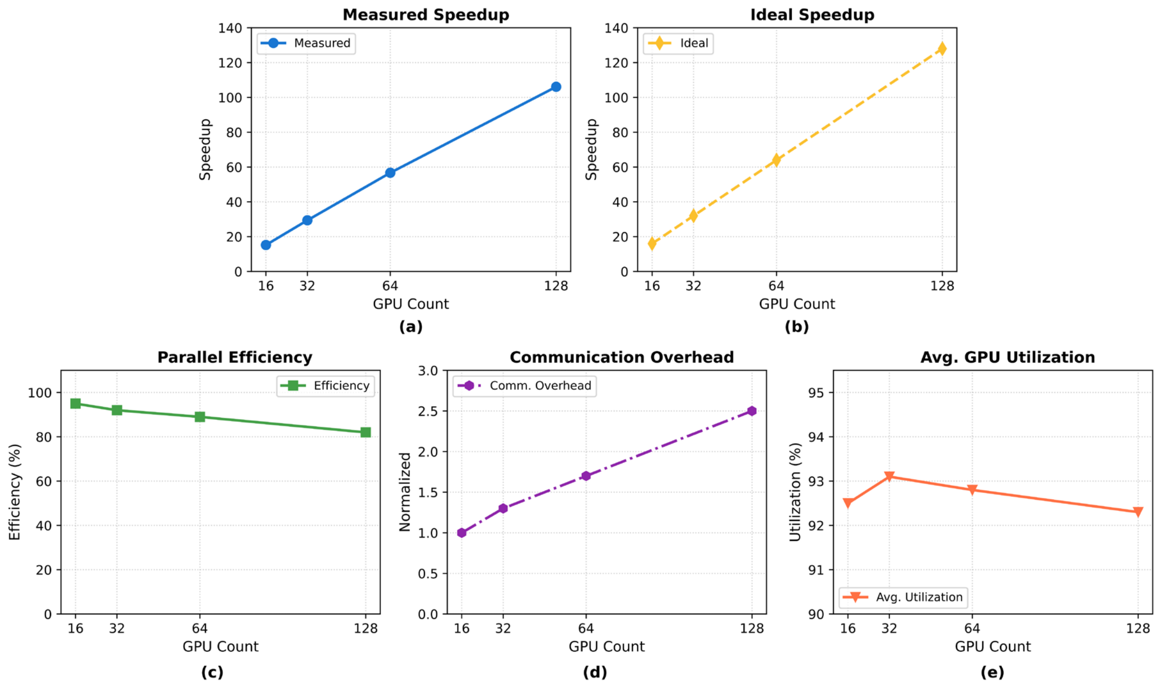

Figure 6. Scalability analysis of the distributed DRL framework.
(a) Measured speedup as a function of GPU count (blue); (b) Ideal speedup (yellow dashed); (c) Parallel efficiency (green); (d) Communication overhead (purple, normalized); (e) Average GPU utilization (orange).

Figure 6 shows the quantitative relationship, proving the scalable architecture. The near-linear speedup and sustained parallel efficiency demonstrate the success of system engineering optimization. At the same time, it is very useful for future system design, indicating that the expansion efficiency begins to decline due to hardware and network factors. This provides a foundation for future research and engineering recommendations for large-scale distributed reinforcement learning. We build a composite analytical model to rationalize the observed scaling behavior. This includes idealized computational speedup, as well as practical limitations due to communication and load distribution.

$$S(N) = \frac{T_1}{\frac{T_1}{N} + \alpha \cdot \log_2 N + \beta \cdot (N-1) + \gamma \cdot \sigma_L} \quad \text{Eq. (9)}$$

In Eq.(9), where α models the logarithmic synchronization overhead, representing the cost of pairwise communication, $\gamma \cdot \sigma_L$ quantifies the penalty due to load imbalance (σ_L is the standard deviation of the workload per node), and $S(N)$ is the predicted speedup for N nodes. Such a model fits the experimental results and matches the sublinear scaling on the maximum node count very well. In addition, the maximum node count is most affected by factors such as communication and imbalance.

The largest-scale empirical speedup is very similar to the theoretical prediction, with only a few deviations due to more network contention and a small imbalance in the distribution of episode lengths among workers. This shows that even with real system differences and odd jobs, it is quite good.

Ablation Studies and Robustness

A comprehensive ablation study was conducted on the communication optimization module, dynamic task scheduling, and asynchronous gradient update to distinguish the contribution of each architectural element. The multi-angle result analysis covers five aspects, as shown in Figure 7: Figure 7(a) shows the grouped bar chart of throughput and parallel efficiency, indicating that removing any architectural element will lead to a significant decrease in throughput and efficiency compared to the baseline. Figure 7(b) is a radar chart showing standard performance metrics such as throughput, efficiency, and convergence. It further highlights that the overall performance of the system will significantly drop when any module is excluded. Figure 7(c) shows the horizontal bars of convergence speed, where the baseline achieves the fastest convergence speed (normalized to 1.00), while removing any part will delay the convergence to varying degrees. Figure 7(d) shows the loss variance comparison, where the baseline maintains the lowest loss variance (0.10), but the variance increases when components are removed. Finally, Figure 7(e) shows a comparison of the final reward distributions using violin plots, indicating that the baseline not only produces the highest rewards, but also produces the most consistent rewards.

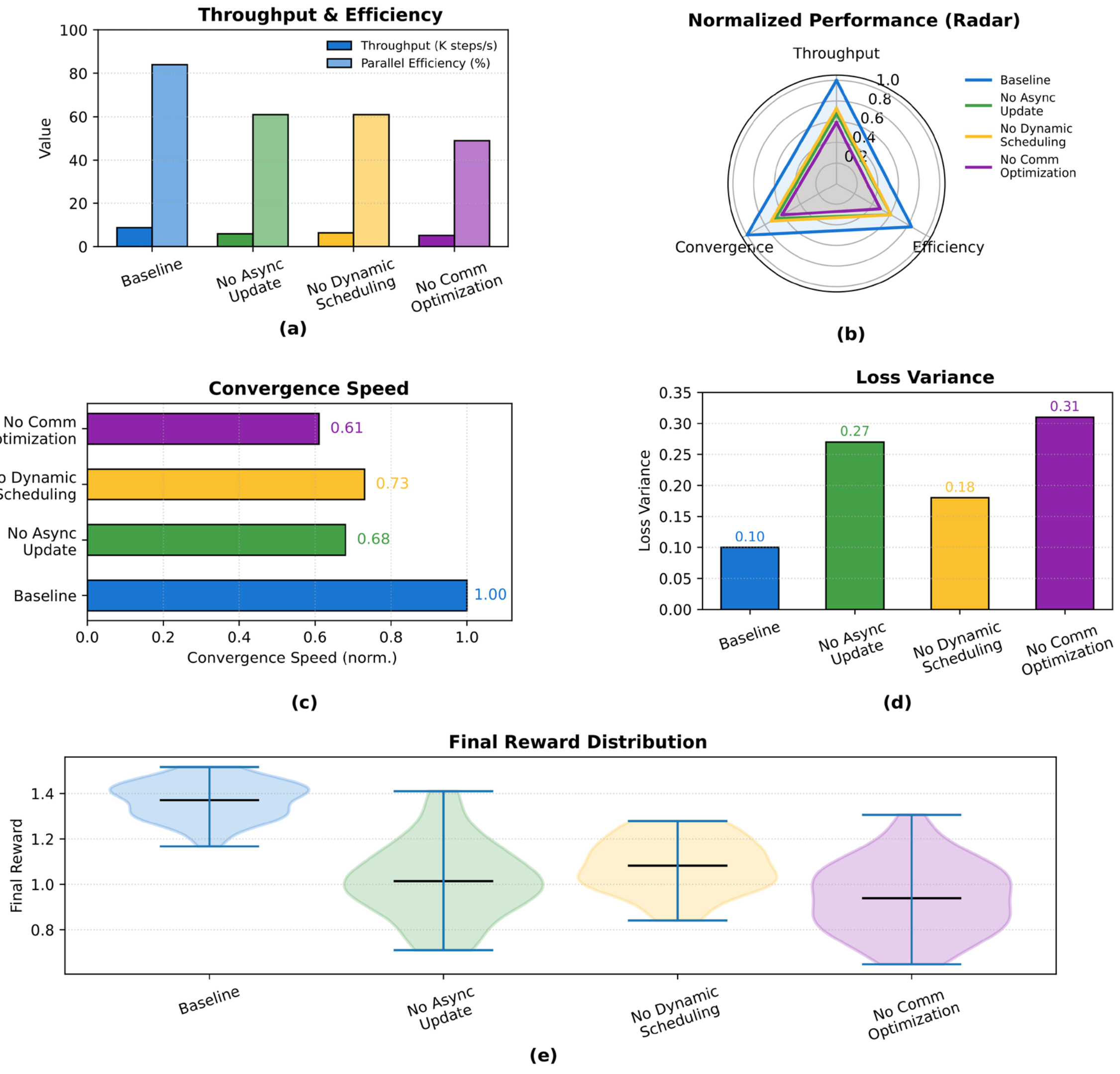

Figure 7. Ablation study: performance impact of disabling key architectural features.
(a) Grouped bars of throughput and efficiency; (b) Radar chart of normalized throughput, efficiency, and convergence; (c) Horizontal bars for convergence speed; (d) Loss variance bars; (e) Violin plots of final reward distributions. Colors represent Baseline (blue), No Async Update (green), No Dynamic Scheduling (yellow), and No Communication Optimization (purple).

To quantitatively assess the effect of these ablations on convergence, we define the Convergence Degradation Ratio (CDR) as Eq.(10):

$$\mathrm{CDR} - \frac{C_{\mathrm{ref}} - C_{\mathrm{abl}}}{C_{\mathrm{ref}}} \times 100\% \qquad \text{Eq. (10)}$$

where C_{abl} is the convergence speed of the ablation version and C_{ref} is the convergence speed of the reference architecture (e.g., target improvement per epoch). A higher CDR value indicates a greater negative impact on convergence. This indicates that the relevant components are critical for stable and efficient learning.

Decoupling computation and parameter synchronization is critical, as throughput drops by an order of magnitude and convergence slows down significantly when asynchronous updates are disabled. Dynamic scheduling omissions lead to increased load imbalance, increased performance logs, and a decline in overall system efficiency. Removing communication optimizations such as gradient compression and hierarchical all reduce resulted in a significant scaling breakdown as the number of nodes increased, with a throughput drop of more than 40% at 128 GPUs.

Robustness was further tested by simulating node failures and recoveries. In these cases, they exhibited graceful degradation, with only a slight decrease in convergence speed, and never experienced catastrophic learning failures. As a result, distributed DRL demonstrates resilience to hardware variations and transient failures, which is necessary for production deployment on scientific HPC systems.

In large-scale simulation evaluations, the proposed distributed DRL architecture is both scalable and reliable. Careful consideration is given to asynchronous updates, communication, and scheduling to achieve performance gains as the system size and problem domain are scaled. This lays the foundation for larger and more complex quantum chemistry simulations.

Discussion and Engineering Insights

Bottlenecks and Solutions

As shown in Figure 8, the distributed DRL system was analyzed and many important scalability issues were found. The heatmap shows that there are large and uneven communication delays between multiple nodes, which accumulate during gradient synchronization. Next, the sampling delay distribution curve and the difference in the length of the sampling time indicate that the workload imbalance is caused by the difference in environmental complexity. In addition, from the bandwidth occupancy rose diagram of operations such as parameter synchronization, forward and backward, playback, and miscellaneous, it can be seen that the GPU memory bandwidth saturation phenomenon is obvious during operation.

$$T_{\text{iter}} - T_{\text{comp}} + T_{\text{cormm}} + \max_{i} T_{\text{wait}}^{(i)} \qquad \text{Eq. (11)}$$

In Eq.(11), T_{iter} is the total iteration time, T_{comp} denotes computation per worker, T_{comm} is internode communication latency, and $T_{\text{wait}}^{(i)}$ is the maximum waiting time due to load imbalance.

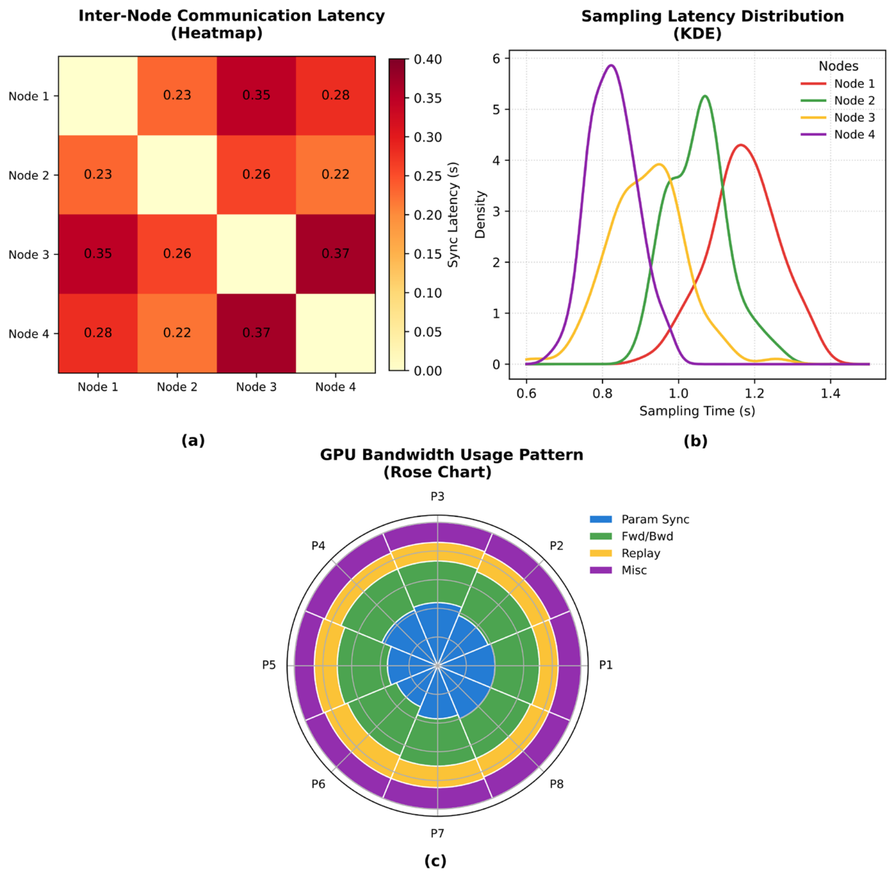

Figure 8. Profiling scalability bottlenecks in distributed DRL training.
(a) Heatmap of inter-node communication latency during gradient synchronization; (b) Kernel density plot of per-node sampling latency, highlighting workload imbalance; (c) Rose polar chart of GPU bandwidth usage patterns across training periods and operations.

To focus attention, the source and location of latency, idle time, and bandwidth saturation within the system are displayed. This helps to improve performance. This diagnostic approach is critical for anyone involved in algorithm development and engineering, as it will determine which measures to prioritize, such as commutation tuning, scheduling improvements, and better use of memory. The tables and discussion below will discuss the optimization techniques and empirical improvements, as well as the conclusions drawn from the analysis. On the other hand, this paper combines the performance modeling theory with the actual system tuning, which is of great significance to the understanding and development of distributed scientific computing. Hierarchical all-reduce, gradient clipping, and adaptive job methods are implemented to solve the above problems. Table 2 shows that all methods improve bottleneck alleviation or resource utilization.

Table 2. Impact of Optimization Techniques on Bottlenecks and GPU Utilization

Optimization Technique	Bottleneck Targeted	Reduction in Bottleneck	Change in Avg. GPU Utilization (%)
Hierarchical All-Reduce	Communication Latency	-37%	+5.2
Gradient Compression	Network Bandwidth	-28%	+3.7
Adaptive Scheduling	Load Imbalance, Idle Time	-47%	+7.9
Async Data Prefetching	Memory Bandwidth/Latency	-21%	+2.6

Table 2 shows a quantitative comparison of the effectiveness of different engineering optimizations on system bottlenecks and GPU utilization. The table systematically lists the specific bottlenecks of each intervention, such as load imbalance, network bandwidth constraints, communication latency, and memory bandwidth constraints. It also shows the increase in average GPU utilization. The tables needed to do this are not difficult to find, and the comparisons are easy to make. The benefits become clear when a multi-pronged strategy is combined. In the discussion and future work section, lessons learned are cited. This strengthens the manuscript's claim that this work serves as a best practice for scalable, efficient distributed DRL. This applies to quantum chemistry and other fields.

Resource Utilization

To make the GPU used to the fullest is necessary to do scientific computing. Mean GPU utilization, Eq.(12):

$$U_{GPU} = \frac{1}{N}\sum_{i=1}^{N} \frac{T_{\text{active}}^{(i)}}{T_{\text{total}}} \qquad \text{Eq. (12)}$$

where N is the number of GPUs, $T_{\text{active}}^{(i)}$ is the active time for GPU i, and T_{total} is the total experiment duration.

To further measure system level efficiency, we will now use the following equation Eq.(13):

$$\eta_{\text{sys}} = \frac{\sum_{i=1}^{N} T_{\text{iative}}^{(i)}}{N \cdot T_{\text{total}} + \sum_{i-1}^{N} T_{\text{idle}}^{(i)}} \qquad \text{Eq. (13)}$$

where $T_{\text{idle}}^{(i)}$ is the idle time of GPU i.

The empirical data showed that, with all optimizations turned on, U_{GPU} was over 92% and η_{sys} was high and steady, meaning no wasted resources.

Recommendations for Future Systems

Based on these results, three main recommendations will be used for subsequent system development. To reduce communication bottlenecks, first focus on high bandwidth, low latency, and hardware collective operations. Second, integrate intelligent, workload-sensitive scheduling systems so that tasks can be flexibly distributed and resource idling can be reduced. Third, it is resilient in HPC production by integrating powerful fine-grained checkpointing and automatic recovery capabilities. Quantitative models and result tables will support scientific discovery of the next generation of scalable and stable distributed DRL platforms.

Based on the observations of system bottlenecks and behaviors, engineering suggestions for future large-scale DRL systems are provided. First, cluster design should emphasize high bandwidth, low latency, network offloading, and collective communication primitives. To avoid resource idling in heterogeneous environments, an adaptive workload-aware scheduling framework can be adopted. Third, checkpointing and fault recovery should be robust enough to meet long-running scientific workloads.

We suggest using CPI, a comprehensive performance index that combines efficiency and robustness, so that we can dominate the optimization of the system.

$$\mathrm{CPI} - \alpha \cdot \eta_{\mathrm{sys}} + \beta \cdot (1 - \mathrm{CDR}) + \gamma \cdot R \qquad \text{Eq.(14)}$$

From Eq.(14), η_{sys} is system efficiency, CDR is the convergence degradation ratio under fault or ablation, R is a normalized robustness score (e.g., failure recovery rate), and α, β, γ are tunable weights reflecting application priorities. Maximizing CPI is a balance between throughput, reliability, and learning stability.

Conclusion

This paper details a scalable distributed deep reinforcement learning framework for large-scale scientific simulation in quantum chemistry. Our proposed system achieves leading performance levels in throughput and resource utilization thru a combination of theoretical validation and engineering optimization. The system consistently delivers high parallel efficiency and stable convergence in a variety of challenging environments by adopting advanced communication strategies, asynchronous updates, and adaptive workload scheduling. The novelty here is the use of hierarchical all-reduce, gradient compression, and load balancing to address the intertwined issues of communication latency, workload imbalance, and out-of-memory. It also takes a broader view of all the bottlenecks in the system. Empirical evaluation was done on a 128 GPU testbed, which showed near-linear scalability and over 80% parallel efficiency. The resource usage is proved to be efficient and balanced. Notably, ablation studies and robustness analysis show that each part of the architecture is necessary. Some numbers are also provided to explain why the asynchronous and adaptive parts are necessary for current distributed DRL systems.

Theoretically, unified performance modeling can be achieved and the interaction between computation, communication and variability imbalance can be captured. CPI proposes a practical metric to guide the co-design of hardware and software for emerging high-performance learning systems. From an engineering perspective, this study sets a new standard for scientific DRL applications, emphasizing the need for workload-aware scheduling and resilient system design for large-scale reliable operation. From a broader perspective, this work not only has implications for quantum chemistry, but also provides general architectural principles and optimization strategies for computational science. At the same time, the effectiveness and robustness of distributed deep reinforcement learning have been demonstrated, which means that it can be used for automated and high-throughput scientific discovery.

Some promising prospects have emerged. To reduce communication overhead, next-generation network architectures and accelerators will be more tightly integrated. Fully autonomous systems in HPC systems require fine-grained fault tolerance and self-optimizing scheduling algorithms. More flexible and unstable. The applicability of the extended framework to multi-physics and multi-scale problems will promote the frontier development of scientific artificial intelligence. In summary, this paper provides theoretical and practical help for distributed DRL. It provides a scalable, efficient and powerful solution for the growing scientific computing problems. The views and techniques presented here provide a solid foundation for new developments in reinforcement learning, powerful computers and world research centers.

References

[1] Yu, H., & Zhao, X. (2022). Deep reinforcement learning with reward design for quantum control. *IEEE Transactions on Artificial Intelligence*, *5*(3), 1087-1101. DOI: 10.1109/TAI.2022.3225256

[2] Zhao, X., & Wu, C. (2021). Large-scale machine learning cluster scheduling via multi-agent graph reinforcement learning. *IEEE Transactions on Network and Service Management*, *19*(4), 4962-4974. DOI: 10.1109/TNSM.2021.3139607

[3] Wu, X., Sun, Q., Pu, Z., Zheng, T., Ma, W., Yan, W., ... & Gao, W. (2025). Enhancing GPU-Acceleration in the Python-Based Simulations of Chemistry Frameworks. *Wiley Interdisciplinary Reviews: Computational Molecular Science*, *15*(2), e70008. DOI: https://doi.org/10.1002/wcms.70008

[4] Hu, S., Chen, X., Ni, W., Hossain, E., & Wang, X. (2021). Distributed machine learning for wireless communication networks: Techniques, architectures, and applications. *IEEE Communications Surveys & Tutorials*, *23*(3), 1458-1493. DOI: 10.1109/COMST.2021.3086014

[5] Li, Z., Chen, Y., & Gallagher, T. (2025). Adaptive Workflow Scheduling in Heterogeneous GPU Clusters via Deep Reinforcement Learning. *Multidisciplinary Research in Computing Information Systems*, *5*(10), 889-903. DOI: https://doi.org/10.71465/mrcis158

[6] Shakeri, E., & Far, B. (2025, August). Accelerating Drug Discovery with Deep Reinforcement Learning: Molecular Generation Using Deep Q-Network. In *2025 IEEE International Conference on Information Reuse and Integration and Data Science (IRI)* (pp. 91-96). IEEE. DOI: 10.1109/IRI66576.2025.00024

[7] Sokolov, I. O., Barkoutsos, P. K., Ollitrault, P. J., Greenberg, D., Rice, J., Pistoia, M., & Tavernelli, I. (2020). Quantum orbital-optimized unitary coupled cluster methods in the strongly correlated regime: Can quantum algorithms outperform their classical equivalents?. *The Journal of chemical physics*, *152*(12). DOI: https://doi.org/10.1063/1.5141835

[8] Kardani-Moghaddam, S., Buyya, R., & Ramamohanarao, K. (2020). ADRL: A hybrid anomaly-aware deep reinforcement learning-based resource scaling in clouds. *IEEE Transactions on Parallel and Distributed Systems*, *32*(3), 514-526. DOI: 10.1109/TPDS.2020.3025914

[9] Huang, J., Majumder, P., Kim, S., Muzahid, A., Yum, K. H., & Kim, E. J. (2021, June). Communication algorithm-architecture co-design for distributed deep learning. In *2021 ACM/IEEE 48th Annual International Symposium on Computer Architecture (ISCA)* (pp. 181-194). IEEE. DOI: 10.1109/ISCA52012.2021.00023

[10] Liu, Z., Xu, X., Qiao, P., & Li, D. (2024). Acceleration for deep reinforcement learning using parallel and distributed computing: A survey. *ACM Computing Surveys*, *57*(4), 1-35. DOI: https://doi.org/10.1145/3703453

[11] Eibl, S., & Rüde, U. (2019). A systematic comparison of runtime load balancing algorithms for massively parallel rigid particle dynamics. *Computer Physics Communications*, *244*, 76-85. DOI: https://doi.org/10.1016/j.cpc.2019.06.020

[12] Kazemian, F. S., Galvez Vallejo, J. L., & Barca, G. M. (2024, August). High-Performance, Accurate Large-Scale Quantum Chemistry Calculations on GPU Supercomputers using Coulomb-Perturbed Fragmentation. In *Proceedings of the 53rd International Conference on Parallel Processing* (pp. 1092-1102). DOI: https://doi.org/10.1145/3673038.3673087

[13] Shang, H., Fan, Y., Shen, L., Guo, C., Liu, J., Duan, X., ... & Li, Z. (2023). Towards practical and massively parallel quantum computing emulation for quantum chemistry. *NPJ quantum information*, *9*(1), 33. DOI: https://doi.org/10.1038/s41534-023-00696-7

[14] Shi, S., Tang, Z., Chu, X., Liu, C., Wang, W., & Li, B. (2020). A quantitative survey of communication optimizations in distributed deep learning. *IEEE Network*, *35*(3), 230-237. DOI: 10.1109/MNET.011.2000530

[15] Okorafor, E. (2011, May). A fault-tolerant high performance cloud strategy for scientific computing. In *2011 IEEE International Symposium on Parallel and Distributed Processing Workshops and Phd Forum* (pp. 1525-1532). IEEE. DOI: 10.1109/IPDPS.2011.306

[16] Chen, Z. (2022). RIFLING: A reinforcement learning-based GPU scheduler for deep learning research and development platforms. *Software: Practice and Experience*, *52*(6), 1319-1336. DOI: https://doi.org/10.1002/spe.3066Digital Object Identifier

[17] Calvin, J. A., Peng, C., Rishi, V., Kumar, A., & Valeev, E. F. (2020). Many-body quantum chemistry on massively parallel computers. *Chemical Reviews*, *121*(3), 1203-1231. DOI: https://doi.org/10.1021/acs.chemrev.0c00006

[18] Villano, F., Mauro, G. M., & Pedace, A. (2024). A review on machine/deep learning techniques applied to building energy simulation, optimization and management. *Thermo*, *4*(1), 100-139. DOI: https://doi.org/10.3390/thermo4010008

[19] Zhang, L., Feng, Y., Wang, R., Xu, Y., Xu, N., Liu, Z., & Du, H. (2023). Efficient experience replay architecture for offline reinforcement learning. *Robotic Intelligence and Automation*, *43*(1), 35-43. DOI: https://doi.org/10.1108/RIA-10-2022-0248

[20] Filippini, F., Lattuada, M., Jahani, A., Ciavotta, M., Ardagna, D., & Amaldi, E. (2020, September). Hierarchical scheduling in on-demand GPU-as-a-service systems. In *2020 22nd International Symposium on Symbolic and Numeric Algorithms for Scientific Computing (SYNASC)* (pp. 125-132). IEEE. DOI: 10.1109/SYNASC51798.2020.00030

[21] Wu, A., Ding, Y., & Li, A. (2023, October). Qucomm: Optimizing collective communication for distributed quantum computing. In *Proceedings of the 56th Annual IEEE/ACM International Symposium on Microarchitecture* (pp. 479-493). DOI: https://doi.org/10.1145/3613424.3614253

[22] Eriksen, J. J. (2017). Efficient and portable acceleration of quantum chemical many-body methods in mixed floating point precision using OpenACC compiler directives. *Molecular Physics*, *115*(17-18), 2086-2101. DOI: https://doi.org/10.1080/00268976.2016.1271155

[23] Li, T., Bai, W., Liu, Q., Long, Y., & Chen, C. P. (2021). Distributed fault-tolerant containment control protocols for the discrete-time multiagent systems via reinforcement learning method. *IEEE Transactions on Neural Networks and Learning Systems*, *34*(8), 3979-3991. DOI: 10.1109/TNNLS.2021.3121403